Applied Surface Science Advances 6 (2021) 100132

Contents lists available at ScienceDirect

Applied Surface Science Advances

journal homepage: www.sciencedirect.com/journal/applied-surface-science-advances

# Active participation of "inert" YSZ substrates on interface formation in $Fe_3O_4$/YSZ heterostructures

Mai Hussein Hamed [*,a,b,*], David N. Mueller [a], Martina Müller [c]

[a] Peter-Grünberg-Institut (PGI-6), Forschungszentrum Jülich GmbH, Jülich 52425, Germany
[b] Faculty of Science, Helwan University, Cairo 11795, Egypt
[c] Faculty of Physics, University of Konstanz, Konstanz 78457, Germany

ARTICLE INFO

*Keywords:*
Verwey transition
HAXPES
YSZ
Redox reaction
$Fe_3O_4$

ABSTRACT

The bulk and emerging interface properties of magnetite $Fe_3O_4$/YSZ(001) heterostructures grown by pulsed laser deposition are investigated. $Fe_3O_4$ thin films (4–38 nm) grow epitaxially in (111) orientation and undergo a Verwey transition at max. $T_V$ = 117±0.6K. Surprisingly, the formation of interfacial $Fe_2O_3$ phase is observed albeit the quasi-inert properties of yttrium-stabilized zirconia (YSZ). Possible mechanisms include either (i) thermodynamically induced interfacial redox reaction at the YSZ substrate surfaces or (ii) oxygen diffusion from the outside atmosphere, as YSZ is a very good oxygen ion conductor. Hence, substrate-assisted oxygen supply may enable the control of emerging interface functionalities.

## 1. Introduction

The atomic scale growth control of complex oxide thin films and heterostructures is essential for realizing advanced oxide electronic applications. Recent developments in high quality oxide growth allowed studying emergent physical properties at oxide interfaces, such as variable conductivity, magnetism or ferroelectricity [1–5]. The ability to create and even tune interface functionalities motivates the search of novel design schemes for oxide heterostructures [6,7]. The overall challenge is to find appropriate ways to control the oxygen content in thin oxide films and at their interfaces, which in turn allow to set their respective functional properties at will.

Iron oxide thin films are promising candidates for application in spin-based oxide electronics due to their variable magnetic properties and conductivity [8–11]. For example, magnetite $Fe_3O_4$ consists of a mixture of $Fe^{3+}$ and $Fe^{2+}$ cations occupying the tetrahedral and octahedral sites of an inverse spinel lattice, and reveals simultaneously ferrimagnetic and electrically half metallic properties. The ferrimagnetic state persist up to a high Curie temperature of $T_C$ = 860K, while the conductivity undergoes an insulator-to-metal (Verwey) transition at $T_V$ = 120K [12,13]. However, it had become evident that the properties of $Fe_3O_4$ ultrathin films are not only controlled by the particular growth conditions but are strongly dependent on the choice of the substrate material [14,15]. Various previous studies report on a – mostly unintentional – formation of either reduced [16,17] or oxidized [18] phases at substrate–film interfaces.

Recently, we demonstrated that the interactions between substrate and $Fe_3O_4$ ultrathin films can stabilize functional iron oxide phases far from equilibrium which otherwise are not accessible by the standard synthesis routes. In particular, we investigated the impact of $SrTiO_3$ substrates on the resulting properties of ultrathin $Fe_3O_4$ films [18] and observed the formation of a 2 u.c. intralayer of ferrimagnetic and insulating $\gamma$-$Fe_2O_3$. An interfacial redox process promotes the transport of oxygen ions from the $SrTiO_3$substrate towards $Fe_3O_4$. Moreover, the thermal activation of the mobility of the oxygen leads to a phase transformations between $Fe_3O_4$, $\gamma$-$Fe_2O_3$ and FeO ultrathin iron oxide films.

In this study, we investigate $Fe_3O_4$ thin films interfaced to YSZ(100), which is a transparent non-magnetic insulator at room temperature, but has considerable ionic conductivity at elevated temperatures. The goal is to elucidate the impact of YSZ(100) substrates on the bulk and emerging interfacial magnetic, structural and physicochemical properties. YSZ shows a much higher resilience to reduction than $SrTiO_3$. Hence, it is often considered as quasi-inert substrate with negligible film-substrate interaction.

* Corresponding author Presentaddress: Jülich Centre for Neutron Science JCNS2 and Peter Grüberg Institut PGI4, JARA-FIT, Forschungszentrum Julich GmbH, 52425, Julich, Germany
*E-mail addresses:* m.hussein@fz-juelich.de (M.H. Hamed), martina.mueller@uni-konstanz.de (M. Müller).

https://doi.org/10.1016/j.apsadv.2021.100132
Received 29 March 2021; Received in revised form 7 June 2021; Accepted 25 June 2021
Available online 7 July 2021

## 2. Experimental details

A series of $Fe_3O_4$ thin films was grown by pulsed laser deposition (PLD) on yttria-stabilized zirconia (001) (YSZ) substrates with 9.5% $Y_2O_3$ doping level. The oxygen partial pressure was kept at $2 \times 10^{-6}$mbar. The laser fluence was set to 1.5 J/cm$^2$ with a repetition rate of 5Hz producing ionized particles from a $Fe_2O_3$rotating target. Here, we vary two growth parameters: the growth temperature ($T_{growth}$ = 300°-500°) and the film thickness ($d$ = 4–38 nm).

The crystalline structure, film thickness and surface roughness of the as-grown $Fe_3O_4$ films were examined using X-ray diffraction (XRD) and X-ray reflectivity (XRR). Both, XRR and XRD experiments were performed at room temperature on a Philips XPert MRD using Cu-$K_\alpha$-radiation. Magnetic properties, i.e. saturation magnetization and Verwey transition of the $Fe_3O_4$/YSZ heterostructures were investigated by a vibrating sample magnetometer (VSM) using a Quantum Design Dynacool physical properties measurement system (PPMS). Magnetic moment versus temperature $M(T)$ was measured in zero-field cooling (ZFC) mode with 500 Oe applied field. Hysteresis loops were recorded at a magnetic field of $H = \pm 5$T along the in-plane [100]-axis.

Element-selective and depth-dependent chemical information of the films and buried interfaces were analyzed by hard X-ray photoelectron spectroscopy (HAXPES) [19] at the KMC-1 beamline at BESSY II (Berlin, Germany) using the HIKE endstation. The photon energy used in this study is $h\nu = 4$ keV which results in an information depth of $\lambda$ = 20–25 nm for $Fe_3O_4$ [20,21]. The samples are adjusted to normal emission geometry.

## 3. Growth temperature: structural and magnetic characterization

### 3.1. Structural properties

First, we study the effect of growth temperature on the structural properties of $Fe_3O_4$ thin films. Using XRD, we performed out-of-plane $\theta - 2\theta$ scans ranging from 15° to 110°, not shown here. All XRD intensities are normalized to their YSZ (002) reflection. In addition to the two peaks corresponding to the YSZ (002) and (004) reflections, we observe four peaks which represent the $Fe_3O_4$ (111), (222), (333) and (444) reflections. These reflections confirm the out-of-plane growth of $Fe_3O_4$ (111) on YSZ (001). The lattice constant of $Fe_3O_4$ is 8.395 Å [22] and of YSZ equals 5.16 Å [23], and the interplanar spacing $d_{(111)}$ of $Fe_3O_4$ is 4.846Å. Therefore, the mismatch between the YSZ (100) and $Fe_3O_4$ (111) is +6%. This can explain the preference of the $Fe_3O_4$ thin films to grow parallel to the (111) planes on the YSZ (100).

Fig. 1 shows the out-of-plane $\theta - 2\theta$ scans of the $Fe_3O_4$ (222) and YSZ (002) reflections. For the films grown at temperatures of 500° and 400°, the $Fe_3O_4$ (222) peak positions are very close to the bulk position of $Fe_3O_4$. However, for the film grown at a temperature of 300°, the peak position is slightly shifted to smaller angles. The calculated out-of-plane lattice constant $c_{oop}$ of all the films is very close to the $Fe_3O_4$ bulk value, where $d_{(111)}$ of the films grown at 500° and 400° is 4.849 Å and for the film grown at 300° equals 4.864 Å. This indicates that all films grow fully relaxed on the YSZ substrates. Moreover, the appearance of the Laue oscillations of the (222) $Fe_3O_4$ reflections reflects the high crystallinity of the films in addition to the structural homogeneity of the films and low density of defects [24].

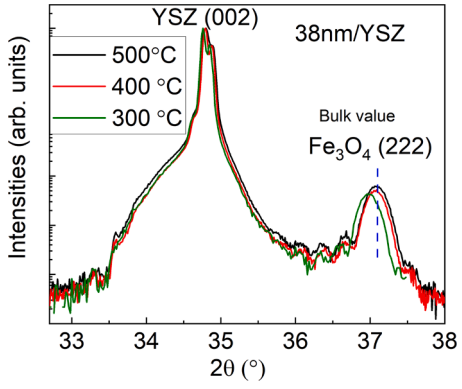


**Fig. 1.** Out-of-plane $\theta - 2\theta$ scans of the $Fe_3O_4$ (222) and the YSZ (002) reflections for 38 nm thick films grown at different growth temperatures $T_{growth}$ = 500°, 400° and 300°.

### 3.2. Saturation magnetization

Next, we study the effect of growth temperature on the magnetic properties of $Fe_3O_4$ thin films. Hysteresis loops have been measured by VSM in order to determine the saturation magnetization of the $Fe_3O_4$ films. Hysteresis loops recorded at temperatures between 5 K and room temperature are depicted in Fig. 2 (a–c). We investigate the saturation magnetization as an important parameter to quantify the magnetic properties of $Fe_3O_4$ films. The saturation magnetization of all $Fe_3O_4$ films is similar within the respective errors (3.3–3.4 $\mu_B$/f.u.). The saturation magnetization is less than the ideal theoretical bulk $Fe_3O_4$ value of 4 $\mu_B$/f.u. [25], which could be due to the formation of antiferromagnetic anti-phase boundaries and structural dislocations. Moreover, the coercivity of all the films grown at different temperatures increases due to the structural transition below the Verwey transition from cubic to monoclinic [26]. The slight differences can be explained by the formation of dislocations and anti-phase boundaries.

### 3.3. Verwey transition

Another approach to characterize the stoichiometry of the $Fe_3O_4$ film is the Verwey transition. The Verwey temperature $T_V$ is strongly influenced by the oxygen content. If $\delta > 0.045$ for nonstoichiometric $Fe_{3-\delta}O_4$, the Verwey transition could not be detected [27,28]. Additionally, $T_V$ is influenced by many parameters like the growth conditions, substrate choice and film thicknesses [29–36]. We can detect the Verwey transition by measuring the magnetization vs. temperature curve. Below the Verwey transition, a transition from cubic structure to a lower symmetry monoclinic phase occurs. This transition causes a decrease of the magnetization at temperature lower than the Verwey transition. Fig. 2 (d–f) depicts the $M(T)$ curve of the films grown at different temperatures. The $M(T)$ curves were measured in zero-field cooling mode with an applied field of 500Oe. In Fig. 2 (d–f), the solid black square represent the magnetization as a function of temperature $M(T)$ of the $Fe_3O_4$ films, which drops around 120 K corresponding to the Verwey transition. The maximum $\partial M/\partial T$ (open red square) and the transition width $\Delta T_V$ (the sharpness of the transition) are calculated in order to exactly determine the Verwey transition $T_V$ and the transition width $\Delta T_V$, respectively. All $Fe_3O_4$ films show almost identical $M(T)$ curves but the magnetic properties in particular the Verwey transition of the $Fe_3O_4$ film grown at $T_{growth}$ = 400° is the closest to the ideal bulk properties. The magnetization of this $Fe_3O_4$ film drops by 17% at the Verwey transition of $T_V = 117 \pm 0.6$ K. In addition, the transition width $\Delta T_V$ of this film equals 14±0.7K. For the films grown at $T_{growth}$ = 500° and $T_{growth}$ = 300°, the decrease of $T_V$ and broadening of $\Delta T_V$ can be attributed to the epitaxial strain, growth defects, oxygen content and reduced domain sizes [31,37]. In our work, we suggest that the decrease of $T_V$ and broadening of $\Delta T_V$ are mainly attributed to oxygen content and growth defects. The domain sizes are supposed to increase with the growth temperature, but for film grown at $T_{growth}$ = 500°, the $T_V$ is reduced and $\Delta T_V$ is broadened. Those observations suggested that the film grown at $T_{growth}$ = 400° has the highest quality in terms of oxygen content. In Table 1, the values of $T_V$ and $\Delta T_V$ of the $Fe_3O_4$ films grown at different temperatures are depicted.

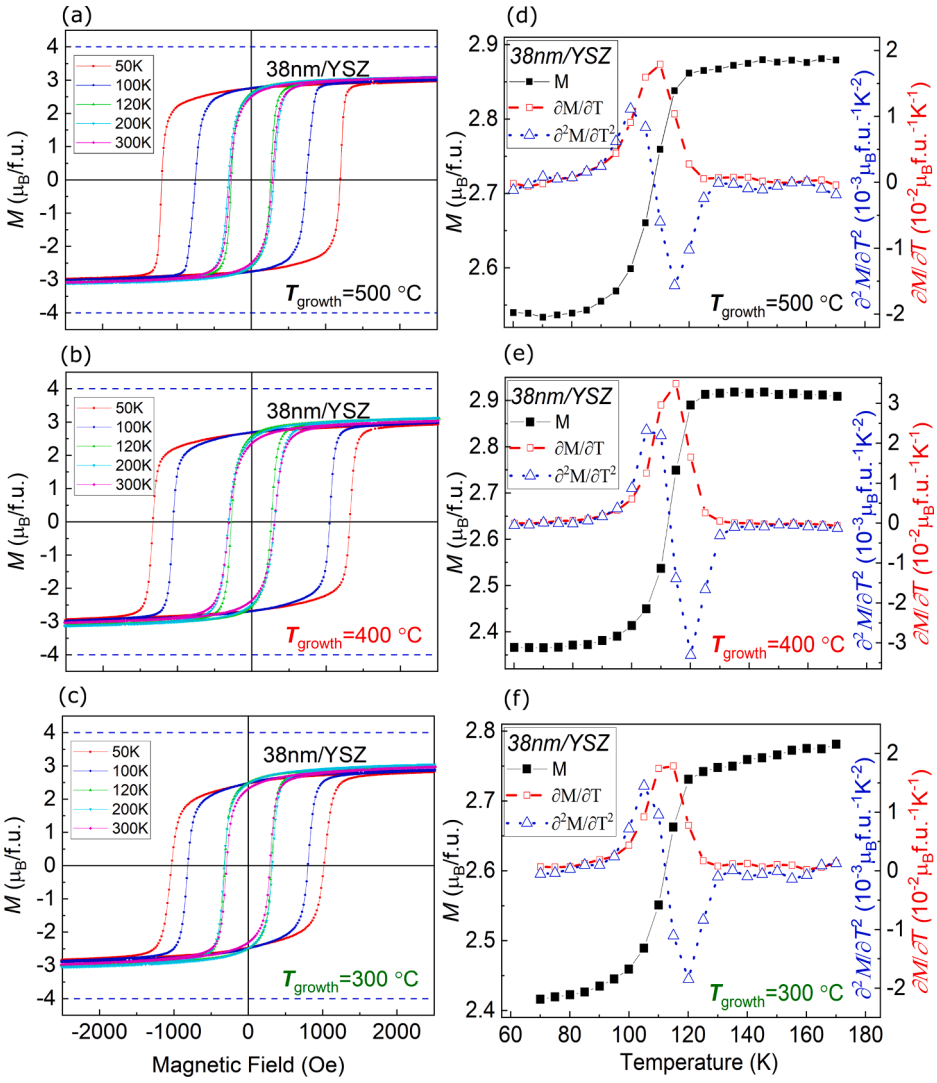


**Fig. 2.** Hysteresis loops for 38nm thick $Fe_3O_4$ films grown at different growth temperatures of (a) 500°, (b) 400°, and (c) 300°. Magnetization vs. temperature (solid square), the first and second derivatives for the magnetization curve (open square and open triangle respectively) of $Fe_3O_4$ films grown at temperatures (d) 500°, (e) 400°, and (f) 300°.

**Table 1**
Magnetization parameters of $Fe_3O_4$/YSZ heterostructures grown at different growth temperatures determined from the $M(T)$ curves.

| $T_{growth}$ (°) | $T_V$ (K) | $\Delta T_V$ (K) | Magnetization drop (%) |
|---|---|---|---|
| 300 | 115±0.8 | 15±0.9 | 12 |
| 400 | 117±0.6 | 14±0.7 | 17 |
| 500 | 113±0.8 | 16±0.8 | 13 |

In summary, for 38nm thick $Fe_3O_4$ films grown on YSZ substrates, the structural properties are independent of the growth temperature. We show that the films are grown parallel to the (111) plane on the YSZ (100) with high crystalline quality indicated by Laue oscillations. However, for the magnetic measurements, there are a slight differences between the films grown with different temperatures, where the $Fe_3O_4$ film grown at $T_{growth} = 400°$ has the closest $T_V$ to the ideal bulk value of 120K. Therefore, we chose the growth temperature of $T_{growth} = 400°$ for the subsequent thickness study.

## 4. Film thickness: physicochemical properties

In the next step, we study the chemical properties of $Fe_3O_4$/YSZ heterostructures and the influence of reduced film thickness down to 4nm. To precisely investigate the stoichiometry of the films, we conducted the bulk element-sensitive HAXPES for $Fe_3O_4$ films of thicknesses between 4 and 38nm grown on YSZ substrates at a growth temperature of 400°.

### 4.1. HAXPES

Fig. 3 (a) shows Fe 2p core level spectra of the 4, 12 and 38 nm thick films. For the 38 nm thick $Fe_3O_4$ film, the two satellites of the $Fe^{2+}$ and $Fe^{3+}$ cations, at binding energies of 715.5 eV and 719 eV [38,39], respectively, are merged. Moreover, in Fig. 3 (b), the Fe $2p_{3/2}$ core level is depicted. The Fe $2p_{3/2}$ core level is composed of the $Fe^{3+}$ peak and a shoulder referring to $Fe^{2+}$. From both observations, a $Fe_3O_4$ bulk-like stoichiometry of the 38 nm thick $Fe_3O_4$ film is confirmed. Similarly, for 12 nm thick film, the two satellites are merged and a slight reduction of the Fe $2p_{3/2}$ peak shoulder intensity are observed. On the other hand, for $d$=4 nm, the $Fe^{3+}$ satellite peak appears and the Fe $2p_{3/2}$ peak shoulder intensity decreases with decreasing film thickness. This

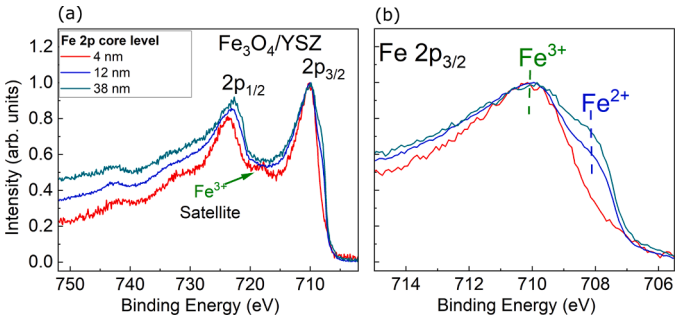


**Fig. 3.** (a) Fe 2p core level spectra of $Fe_3O_4$(111)/YSZ(001) for varying film thicknesses recorded at $h\nu = 4\,keV$. (b) Zoom into the Fe $2p_{3/2}$ core level.

indicates a decrease of the $Fe^{2+}$ contribution and the formation of an $Fe_2O_3$phase in addition to the $Fe_3O_4$ phase.

The observation of the $Fe_2O_3$ phase may indicate an oxygen supply from the underlying YSZ substrate. This possibly causes a redox reaction with the iron oxide films at the interface as we observed also previously for $Fe_3O_4$ films grown on Nb:$SrTiO_3$ [18,40]. We explained the formation of the oxidized $\gamma$-$Fe_2O_3$ phase at the interface by the reduction of the $TiO_2$-terminated $SrTiO_3$substrate, which in turn causes the oxidation of $Fe_3O_4$ to form the $\gamma$-$Fe_2O_3$intralayer. However, in case of YSZ substrate, the reducibility of the YSZ is much lower compared to $SrTiO_3$. Moreover, the oxygen ion conductivity of the YSZ also depends on the doping percentage [41,42]. Therefore, the thermodynamics play an important role as we discuss in the next section.

## 5. Substrate-assisted interface oxidation

From bulk thermodynamics, the formation enthalpies have nearly similar values: the Gibbs free energy $\Delta G_F^o$ equals -1200 kJ/mol [43] and -1164 kJ/mol [44] for YSZ (with $Y_2O_3$ doping level of 10%) and for $Fe_3O_4$, respectively. Therefore, no clear expectation of which phase may be reduced which can be drawn. It should be noted, however, that since YSZ is such a good oxygen ion conductor, any formation of additional oxygen vacancies (concomitant with reduction of Zr) at the interface will be followed by a quick redistribution, making the concentration of excess oxygen vacancies at the interface quite small. Additionally, excess oxygen vacancies can be replenished by oxygen gas from the atmosphere.

Additionally, the YSZ is known to be a good electrolyte because of its high oxygen conductivity [45] which is influenced by the doping level as well [46]. Therefore, oxygen can diffuse from the outer atmosphere through the YSZ substrate and cause the formation of an $Fe_2O_3$ intralayer (Fig. 4). Therefore, the oxygen conductivity of YSZ is a key factor for the formation of an oxidized $Fe_3O_4$ intralayer. However, the perturbation of oxygen vacancy concentration caused by this redistribution within the substrate crystal plays a negligible role.

## 6. Conclusion

In summary, we investigate the bulk and emerging structural, magnetic and physicochemical interface properties of $Fe_3O_4$ thin films ($d$ = 4-38nm) grown on YSZ(001) substrates. All $Fe_3O_4$ thin films grow epitaxially in (111) orientation and reveal Laue oscillations as an indication for high crystalline quality. A Verwey transition was observed for all $Fe_3O_4$/YSZ samples. $T_V = 117\pm0.6$K was found for 38nm $Fe_3O_4$ grown at $T_{growth} = 400^{\circ}$, which is closest to bulk $T_V$. The chemical properties were investigated by HAXPES and surprisingly reveal the formation of a few unit cells (u.c.) $Fe_2O_3$ intralayer in 4nm $Fe_3O_4$/YSZ – although YSZ is considered as a quasi-inert substrate with negligible oxygen diffusivity. The formation of this $Fe_2O_3$ intralayer can be explained by two scenarios: Either (i) a supply of oxygen from the YSZ substrate or (ii) the diffusion of oxygen through the substrate. In the first case, the resulting excess vacancies are distributed fast enough through the whole YSZ substrate, making the amount of excess vacancies very small. In the second scenario, the diffusion of oxygen is possible because YSZ is a very good oxygen conductor. In general, these findings emphasize the complex substrate–film interaction in oxide heterostructures, and the resulting opportunity to control the emerging interface functionalities-even with seemingly inert substrates.

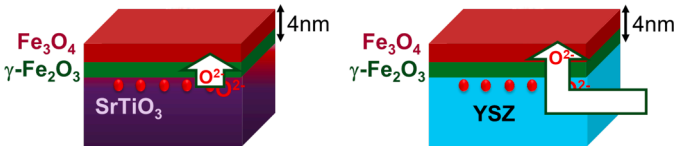


**Fig. 4.** The formation process of $Fe_2O_3$ at the interfaces between the oxides substrates ($SrTiO_3$ and YSZ) and $Fe_3O_4$ films has different mechanisms: (1) redox process at the interfaces $Fe_3O_4/SrTiO_3$ and (2) oxygen diffusion through the substrate from the outer atmosphere into $Fe_3O_4$/YSZ.

## Acknowledgments

We acknowledge R. Dittmann for providing the PLD setup at FZJ as well as O. Petracic and T. Brückel for providing measurement time at VSM at FZJ. We thank R. F. Duarte for his support during the beamtime at HIKE (BESSY II, HZB Berlin). D. N. Mueller gratefully acknowledges support by the Juelich Joint Redox Laboratory (JJRL). M. H. Hamed thanks the Egyptian Ministry of Higher Education for providing a PhD scholarship. M. Müller acknowledges funding by the Deutsche Forschungsgemeinschaft (DFG, German Research Foundation) " SFB 1432 " Project-ID 425217212.

## References

[1] I.V. Maznichenko, S. Ostanin, A. Ernst, I. Mertig, Tunable 2D electron gas at the $LaAlO_3/SrTiO_3$(001) interface, Phys. Rev. Mater. 3 (2019) 074006, https://doi.org/10.1103/PhysRevMaterials.3.074006.
[2] M. Salluzzo, S. Gariglio, D. Stornaiuolo, V. Sessi, S. Rusponi, C. Piamonteze, G. M. De Luca, M. Minola, D. Marré, A. Gadaleta, H. Brune, F. Nolting, N.B. Brookes, G. Ghiringhelli, Origin of interface magnetism in $BiMnO_3/SrTiO_3$ and $laalo_3/SrTiO_3$ heterostructures, Phys. Rev. Lett. 111 (2013) 087204, https://doi.org/10.1103/PhysRevLett.111.087204.
[3] R. Takahashi, Y. Cho, M. Lippmaa, Interfacial capacitance between a ferroelectric $Fe_3O_4$ thin film and a semiconducting nb:$SrTiO_3$ substrate, J. Appl. Phys. 117 (1) (2015) 014104, https://doi.org/10.1063/1.4905384.
[4] P. Lömker, T.C. Rödel, T. Gerber, F. Fortuna, E. Frantzeskakis, P. Le Fèvre, F.M. C. Bertran, M. Müller, A.F. Santander-Syro, Two-dimensional electron system at the magnetically tunable EuO/$SrTiO_3$ interface, Phys. Rev. Mater. 1 (2017) 062001, https://doi.org/10.1103/PhysRevMaterials.1.062001.
[5] G.M. Prinz, T. Gerber, A. Lorke, M. Müller, Quantum confinement in EuO heterostructures, Appl. Phys. Lett. 109 (20) (2016) 202401, https://doi.org/10.1063/1.4966223.
[6] T. Gerber, P. Lömker, B. Zijlstra, C. Besson, D.N. Mueller, W. Zander, J. Schubert, M. Gorgoi, M. Müller, Thermodynamic stability and control of oxygen reactivity at functional oxide interfaces: EuO on ITO, J. Mater. Chem. C 4 (2016) 1813–1820, https://doi.org/10.1039/C6TC00170J.
[7] C. Caspers, A. Gloskovskii, W. Drube, C.M. Schneider, M. Müller, conductive yttria-stabilized zirconia as an epitaxial template for oxide heterostructures, J. Appl. Phys. 115 (17) (2014) 17C111, https://doi.org/10.1063/1.4863803.
[8] H.C. Wu, O.N. Mryasov, M. Abid, K. Radican, I.V. Shvets, Magnetization states of all-oxide spin valves controlled by charge-orbital ordering of coupled ferromagnets. Sci. Rep. 3 (2013) 1830, https://doi.org/10.1038/srep01830.
[9] Z.-M. Liao, Y.-D. Li, J. Xu, J.-M. Zhang, K. Xia, D.-P. Yu, Spin-filter effect in magnetite nanowire, Nano Lett. 6 (6) (2006) 1087–1091, https://doi.org/10.1021/nl052199p.PMID: 16771558
[10] S. Parkin, Xin Jiang, C. Kaiser, A. Panchula, K. Roche, M. Samant, Magnetically engineered spintronic sensors and memory, Proc. IEEE 91 (5) (2003) 661–680.
[11] E. Wada, K. Watanabe, Y. Shirahata, M. Itoh, M. Yamaguchi, T. Taniyama, Efficient spin injection into GaAs quantum well across $Fe_3O_4$ spin filter, Appl. Phys. Lett. 96 (10) (2010) 102510, https://doi.org/10.1063/1.3357436.
[12] M.S. Senn, J.P. Wright, J.P. Attfield, Charge order and three-site distortions in the Verwey structure of magnetite, Nature 481 (2012) 1476–4687, https://doi.org/10.1038/nature10704.
[13] E.J.W. VERWEY, Electronic conduction of magnetite ($Fe_3O_4$) and its transition point at low temperatures, Nature 144 (1939) 327–328, https://doi.org/10.1038/144327b0.

[14] T. Tsuchiya, K. Terabe, M. Ochi, T. Higuchi, M. Osada, Y. Yamashita, S. Ueda, M. Aono, In situ tuning of magnetization and magnetoresistance in $Fe_3O_4$ thin film achieved with all-solid-state redox device, ACS Nano 10 (1) (2016) 1655–1661, https://doi.org/10.1021/acsnano.5b07374.
[15] E. Liu, Y. Yin, L. Sun, Y. Zhai, J. Du, F. Xu, H. Zhai, Increasing spin polarization in $Fe_3O_4$ films by engineering antiphase boundary densities, Appl. Phys. Lett. 110 (14) (2017) 142402, https://doi.org/10.1063/1.4979586.
[16] O. Kuschel, W. Spiess, T. Schemme, J. Rubio-Zuazo, K. Kuepper, J. Wollschlger, Real-time monitoring of the structure of ultrathin $Fe_3O_4$ films during growth on Nb-doped $SrTiO_3$(001), Appl. Phys. Lett. 111 (4) (2017) 041902, https://doi.org/10.1063/1.4995408.
[17] D. Gilks, L. Lari, K. Matsuzaki, H. Hosono, T. Susaki, V.K. Lazarov, Structural study of $Fe_3O_4$(111) thin films with bulk like magnetic and magnetotransport behaviour, J. Appl. Phys. 115 (17) (2014) 17C107, https://doi.org/10.1063/1.4862524.
[18] M.H. Hamed, R.A. Hinz, P. Lömker, M. Wilhelm, A. Gloskovskii, P. Bencok, C. Schmitz-Antoniak, H. Elnaggar, C.M. Schneider, M. Müller, Tunable magnetic phases at $Fe_3O_4$/$SrTiO_3$ oxide interfaces, ACS Appl. Mater. Interfaces 11 (7) (2019) 7576–7583, https://doi.org/10.1021/acsami.8b20625.
[19] M. Müller, S. Nemk, L. Plucinski, C.M. Schneider, Functional materials for information and energy technology: Insights by photoelectron spectroscopy, J. Electr. Spectrosc. Relat. Phenom. 208 (2016) 24–32, https://doi.org/10.1016/j.elspec.2015.08.003.Special Issue: Electronic structure and function from state-of-the-art spectroscopy and theory
[20] S. Tanuma, C.J. Powell, D.R. Penn, Calculations of electron inelastic mean free paths. IX. Data for 41 elemental solids over the 50 eV to 30 keV range, Surf. Interface Anal. 43 (3) (2011) 689–713, https://doi.org/10.1002/sia.3522.
[21] J.A. Coln Santana, Quantitative Core Level Photoelectron Spectroscopy, in: 2053-2571, Morgan and Claypool Publishers, 2015, https://doi.org/10.1088/978-1-6270-5306-8.
[22] M.E. Fleet, The structure of magnetite, Acta Crystallogr. Sect. B 37 (4) (1981) 917–920, https://doi.org/10.1107/S0567740881004597.
[23] H. Horiuchi, A.J. Schultz, P.C.W. Leung, J.M. Williams, Time-of-flight neutron diffraction study of a single crystal of yttria-stabilized zirconia, $Zr(Y)O_{1.862}$, at high temperature and in an applied electrical field, Acta Crystallogr. Sect. B 40 (4) (1984) 367–372, https://doi.org/10.1107/S0108768184002329.
[24] G.K. Pálsson, A.R. Rennie, B. Hjörvarsson, Examination of the reliability of x-ray techniques for determining hydrogen-induced volume changes, Phys. Rev. B 78 (2008) 104118, https://doi.org/10.1103/PhysRevB.78.104118.
[25] WeissPierre, Forrer, R., La saturation absolue des ferromagnétiques et les lois d'approche en fonction du champ et de la température, Ann. Phys. 10 (12) (1929) 279–372, https://doi.org/10.1051/anphys/192910120279.
[26] A. Muxworthy, Low-temperature susceptibility and hysteresis of magnetite, Earth Planet. Sci. Lett. 169 (1) (1999) 51–58, https://doi.org/10.1016/S0012-821X(99)00067-9.
[27] F. Walz, The verwey transition - a topical review, J. Phys. Condens. Matter 14 (12) (2002) R285–R340, https://doi.org/10.1088/0953-8984/14/12/203.
[28] R. Aragón, D.J. Buttrey, J.P. Shepherd, J.M. Honig, Influence of nonstoichiometry on the Verwey transition, Phys. Rev. B 31 (1985) 430–436, https://doi.org/10.1103/PhysRevB.31.430.
[29] C.F. Chang, Z. Hu, S. Klein, X.H. Liu, R. Sutarto, A. Tanaka, J.C. Cezar, N. B. Brookes, H.-J. Lin, H.H. Hsieh, C.T. Chen, A.D. Rata, L.H. Tjeng, Dynamic atomic reconstruction: How $Fe_3O_4$ thin films evade polar catastrophe for epitaxy, Phys. Rev. X 6 (2016) 041011, https://doi.org/10.1103/PhysRevX.6.041011.
[30] J. Orna, P.A. Algarabel, L. Morellón, J.A. Pardo, J.M. de Teresa, R. López Antón, F. Bartolomé, L.M. García, J. Bartolomé, J.C. Cezar, A. Wildes, Origin of the giant magnetic moment in epitaxial $Fe_3O_4$ thin films, Phys. Rev. B 81 (2010) 144420, https://doi.org/10.1103/PhysRevB.81.144420.
[31] X.H. Liu, A.D. Rata, C.F. Chang, A.C. Komarek, L.H. Tjeng, Verwey transition in $Fe_3O_4$ thin films: Influence of oxygen stoichiometry and substrate-induced microstructure, Phys. Rev. B 90 (2014) 125142, https://doi.org/10.1103/PhysRevB.90.125142.
[32] S. Alraddadi, W. Hines, T. Yilmaz, G.D. Gu, B. Sinkovic, Structural phase diagram for ultra-thin epitaxial $Fe_3O_4$/MgO(001) films: thickness and oxygen pressure dependence, J. Phys. Condens. Matter 28 (11) (2016) 115402, https://doi.org/10.1088/0953-8984/28/11/115402.
[33] J.A. Moyer, S. Lee, P. Schiffer, L.W. Martin, Magnetically disordered phase in epitaxial iron-deficient $Fe_3O_4$ thin films, Phys. Rev. B 91 (2015) 064413, https://doi.org/10.1103/PhysRevB.91.064413.
[34] A. Hamie, Y. Dumont, E. Popova, A. Fouchet, B. Warot-Fonrose, C. Gatel, E. Chikoidze, J. Scola, B. Berini, N. Keller, Investigation of high quality magnetite thin films grown on $SrTiO_3$(001) substrates by pulsed laser deposition, Thin Solid Films 525 (2012) 115–120, https://doi.org/10.1016/j.tsf.2012.10.076.
[35] M.B. Yazdi, M. Major, A. Wildes, F. Wilhelm, A. Rogalev, W. Donner, L. Alff, Possible evidence for a spin-state crossover in the verwey state in $Fe_3O_4$ thin films, Phys. Rev. B 93 (2016) 014439, https://doi.org/10.1103/PhysRevB.93.014439.
[36] J. Dho, B.-g. Kim, S. Ki, Distinctive uniaxial magnetic anisotropy and positive magnetoresistance in (110)-oriented $Fe_3O_4$ films, J. Appl. Phys. 117 (16) (2015) 163904, https://doi.org/10.1063/1.4918915.
[37] X.W. Li, A. Gupta, G. Xiao, G.Q. Gong, Transport and magnetic properties of epitaxial and polycrystalline magnetite thin films, J. Appl. Phys. 83 (11) (1998) 7049–7051, https://doi.org/10.1063/1.367547.
[38] T. Fujii, F.M.F. de Groot, G.A. Sawatzky, F.C. Voogt, T. Hibma, K. Okada, In situ XPS analysis of various iron oxide films grown by $NO_2$-assisted molecular-beam epitaxy, Phys. Rev. B 59 (1999) 3195–3202, https://doi.org/10.1103/PhysRevB.59.3195.
[39] S. Gota, E. Guiot, M. Henriot, M. Gautier-Soyer, Atomic-oxygen-assisted MBE growth of $\alpha-Fe_2O_3$ on $\alpha-Al_2O_3$(0001): Metastable FeO(111)-like phase at subnanometer thicknesses, Phys. Rev. B 60 (1999) 14387–14395, https://doi.org/10.1103/PhysRevB.60.14387.
[40] M.H. Hamed, D.N. Mueller, M. Müller, Thermal phase design of ultrathin magnetic iron oxide films: from $Fe_3O_4$ to $\gamma$-$Fe_2O_3$and FeO, J. Mater. Chem. C 8 (2020) 1335–1343, https://doi.org/10.1039/C9TC05921K.
[41] J. Janek, C. Korte, Electrochemical blackening of yttria-stabilized zirconia morphological instability of the moving reaction front, Solid State Ion. 116 (3) (1999) 181–195, https://doi.org/10.1016/S0167-2738(98)00415-9.
[42] B. Savoini, C. Ballesteros, J.E. Muñoz Santiuste, R. González, Y. Chen, Thermochemical reduction of yttria-stabilized-zirconia crystals: optical and electron microscopy, Phys. Rev. B 57 (1998) 13439–13447, https://doi.org/10.1103/PhysRevB.57.13439.
[43] M. Asadikiya, H. Sabarou, M. Chen, Y. Zhong, Phase diagram for a nano-yttria-stabilized zirconia system, RSC Adv. 6 (2016) 17438–17445, https://doi.org/10.1039/C5RA24330K.
[44] M.W. Chase, NIST-JANAF thermochemical tables, in: Journal of physical and chemical reference data., Monograph ; no.9, American Institute of Physics for the National Institute of Standards and Technology, U.S. Department of Commerce: Gaithersburg, MD, 1998.
[45] V.M. Orera, R.I. Merino, Y. Chen, R. Cases, P.J. Alonso, Intrinsic electron and hole defects in stabilized zirconia single crystals, Phys. Rev. B 42 (1990) 9782–9789, https://doi.org/10.1103/PhysRevB.42.9782.
[46] N.Q. Minh, Ceramic fuel cells, J. Am. Ceram. Soc. 76 (3) (1993) 563–588, https://doi.org/10.1111/j.1151-2916.1993.tb03645.x.